ELASTIC SCATTERING OF DEUTERONS FROM O^{16}

David Warren Berger
and
Ollie Joseph Loper

Library
U. S. Naval Postgraduate School
Monterey, California

1-25

DEU - DEUTERON

SCA - SCATTERING

OXY - OXYGEN

Si

Accepted

Thesis

ELASTIC SCATTERING OF DEUTERONS FROM O^{16}

by

David Warren Berger
and
Ollie Joseph Loper

Submitted to the Department of Physics on May 21, 1956 in partial fulfillment of the requirements for the degree of Master of Science.

ABSTRACT

The differential cross section for the elastic scattering of deuterons from O^{16} was measured in the deuteron energy range 4.590 to 7.196 Mev at 130 degrees and from 5.449 to 6.315 Mev at 90 degrees.

The absolute cross section was determined by comparison with the known $O^{16}(p,p)O^{16}$ cross section.

The error of the cross section was computed to be ± 5 percent (standard deviation) at 130 degrees and ± 10 percent (standard deviation) at the 90-degree angle.

As would be expected at this bombarding energy, it has been clearly shown that the cross sections do not follow the Rutherford scattering law but do show marked overlapping resonance structure.

The data were obtained using the MIT-ONR electrostatic generator and the broad-range magnetic spectrograph.

A scintillation counter constructed by the authors was used to record the scattered deuterons.

The response characteristics of a CsI(Tl) crystal were measured for alpha particles, protons, and deuterons.

A comparison with the $O^{16}(d,\alpha)N^{14}$ yield is made.

Supervisor: Cornelius P. Browne

Title: Research Associate in Physics

25738

ACKNOWLEDGMENTS

The authors are indebted to Dr. C. P. Browne for supervision of this thesis and the use of his unpublished work on $O^{16}(d,\alpha)N^{14}$ as an included reference and to Professor W. W. Buechner and Mr. A. Sperduto for their advice and encouragement.

Acknowledgment is given to Dr. F. J. Eppling for his cooperation in permitting the use of his cross-section data.

The authors would like to thank Mr. Wilton Tripp, Miss Sylvia Darrow, and Miss Estelle Freedman for counting the nuclear track emulsions, Mrs. Grace Rowe of the Laboratory for Nuclear Science drafting room for inking the plates, and the members of the High Voltage Laboratory in general for their help in preparation of this thesis.

Particular thanks are due Mrs. Mary E. White for editing and preparation of the final drafts and Mr. E. W. Nickerson for assistance in constructing the counter assembly and other equipment.

TABLE OF CONTENTS

Page Number

I. INTRODUCTION 1

II. EXPERIMENTAL METHOD 3

EQUIPMENT AND PROCEDURE 3

TARGETS 5

Table I. Target Thicknesses 6

III. THE COUNTER SYSTEM AND ITS CHARACTERISTICS 7

IV. REDUCTION OF DATA 13

SUMMARY OF DATA 13

REDUCTION OF YIELD DATA 13

Table II. Summary of Plate Data 14

Table III. Counter Data for Yield Ratios 16

CROSS-SECTION DETERMINATION 17

Table IV. $O^{16}(p,p)O^{16}$ Cross Sections 18

Table V. Cross Sections from Nuclear Track Plates 20

ENERGY DETERMINATION 21

SUMMARY OF DATA REDUCTION AND ERROR DETERMINATIONS 23

V. RESULTS AND CONCLUSIONS 24

Table VI. Observed Maxima in $O^{16}(d,d)O^{16}$ Cross Sections 25

APPENDIX I. NORMALIZED AVERAGE COUNTER DATA AT 130° SPECTROGRAPH ANGLE 29

NORMALIZED AVERAGE COUNTER DATA AT 90° SPECTROGRAPH ANGLE 35

APPENDIX II. COMPUTATION OF DEUTERON CONTAMINATION IN MOLECULAR HYDROGEN BEAM 37

Figure 1. Relative Response of CsI(Tl) Crystal to Protons, Deuterons, and Alpha-particles 39

Figure 2. CsI(Tl) Counter Response versus Elastic Group Position on Crystal 40

Figure 3. Cross Section for Elastic Deuterons from O^{16} at 135.54° and 97.24° (Center of Mass) 41

Figure 4. Cross Section for Elastic Deuterons from O^{16} (Laboratory) 42

Figure 5. $O^{16}(d,\alpha)N^{14}$ Yield Curve 30° (Laboratory) 43

Figure 6. $O^{16}(d,d)O^{16}$ Cross Section Illustrating Broad Resonance Background 44

Figure 7. $O^{16}(d,\alpha)N^{14}$ and $O^{16}(d,d)O^{16}$ Yields Superimposed for Comparison 45

BIBLIOGRAPHY 46

I. INTRODUCTION

The compound nucleus, F^{18}, has been investigated previously by several reactions involving deuterons incident on O^{16}. The highest excitation reached in recent work is 10.9 Mev by Stratton et al (S1) who obtained the absolute cross sections and excitation functions for $O^{16}(d,p)O^{17}$ and $O^{16}(d,p)O^{17*}$. These same reactions have also been observed by Heydenburg and Inglis (H1) up to an excitation of 10.4 Mev. The yield of F^{17} from the reaction $O^{16}(d,n)F^{17}$ has been obtained by Newson (N1) and Bonner (B5) up to an excitation of 11.9 Mev. Newson concluded that the coulomb barrier height for O^{16} + d was 3.1 Mev.

Previous reliable level assignments are given to 10.5-Mev excitation in F^{18} (A1).

Browne (B3)(B4) has examined the reaction $O^{16}(d,\alpha)N^{14}$ and also $O^{16}(d,\alpha)N^{14*}$ from an excitation of 12.4 to 14.2 Mev, obtaining the yield of alpha particles from the ground state, first excited state, and second excited state of N^{14} where the reaction leading to the first excited state in N^{14} is forbidden on the basis of isobaric spin-selection rules, since this level in N^{14} has T = 1 (A1, p. 125). This reaction leads to the formation of the same compound nucleus as the reaction $O^{16}(d,d)O^{16}$.

The reactions $O^{16}(d,\alpha)N^{14}$, N^{14*}, $O^{16}(d,d)O^{16}$, and $N^{14}(\alpha,\alpha)N^{14}$ involve only particles of zero intrinsic isobaric spin, and hence will excite only those levels in F^{18} that have isobaric spin (T = 0) and not levels with T = 1, provided that the isobaric spin-selection

rules hold. Isobaric spin selection, therefore, provides a means of selectively exciting levels when it is valid.

The (d,α) data (B4), Figure 5, do not show discrete level structure but apparently show dense overlapping levels in this region of excitation. It is the purpose of the present experiment to use the elastic scattering of deuterons from O^{16} to investigate the level structure of F^{18} in the region of excitation covered by Browne and then to continue the investigation down to a lower excitation through the transition region where dense overlapping level structure is resolved into well-defined isolated levels where it is possible to determine level spacing, width, and excitation.

It is hoped to determine any correlation between the resonances of the (d,α) data and the (d,d) data.

II. EXPERIMENTAL METHOD

EQUIPMENT AND PROCEDURE

The data were obtained using the MIT-ONR Van de Graaff generator. The generator is a vertical machine that operates in the voltage range of about 4 to 8 Mev. The beam is deflected to the horizontal plane by a deflecting magnet of radius 60.51 cm. The beam is defined at the entrance and exit of the deflecting magnet by pairs of slits of 1 mm and ½ mm aperture, respectively. These apertures, for constant magnetic field in the deflecting magnet, limit the incident beam energy spread to ± 0.10 percent. The exit slits are insulated and connected to a voltage stabilizing device that controls a corona discharge to the generator terminal.

A homogeneous beam of deuterons was scattered from a thin SiO_2 (on Formvar) target, and the elastic deuterons from O^{16} were counted by a scintillation counter mounted at a fixed radius (51.36 cm) in the broad-range magnetic spectrograph (B1). The magnetic spectrograph slit system determines the solid angle of observation, which is 3.6×10^{-4} steradians ± 10 percent for a radius of 51.36 cm. The solid angle is constant in the laboratory system for all spectrograph angles, provided that the illuminated target spot is less than 2 mm in greatest dimension. The total beam current incident on the target is measured by an electronic current integrator (E2) connected to a Faraday cage in the scattering chamber.

The energy of the deuteron beam is varied by adjustment of the magnetic field of the deflecting magnet, which, by means of the voltage stabilizing device, changes the generator voltage to maintain the new energy beam on the target. The incident energy was varied in approximately 20-kev steps (25 kcs on the nuclear magnetic resonance fluxmeter).

The windings in the deflecting magnet and spectrograph are supplied by a stabilized three-phase rectifier circuit that holds the field constant to 1 part in 100,000 (B2). The resultant fields are measured by nuclear magnetic resonance fluxmeters.

With the spectrograph at a fixed angle in the laboratory system, the magnetic field was adjusted to keep the O^{16} elastic deuteron group centered on the scintillation crystal for each input energy.

Raw data of "number of elastic deuterons incident on the crystal per Q_d microcoulombs of incident deuteron beam on target" were obtained versus $B\rho$ (input) for the range 437.94 to 548.56 kilogauss-centimeters. Q_d was chosen such that the yield obtained had a standard deviation less than 5 percent, assuming a Poisson distribution. To reduce the yield data to an absolute cross section, the yield of elastic deuterons was measured relative to the yield of elastic protons for two points on the 130-degree curve. The absolute cross section for $O^{16}(p,p\ )O^{16}$ is known from the work of Eppling (E1). The comparison of relative yields was made, using nuclear track plates in place of the scintillation counter in the magnetic spectrograph.

Critical points on the yield curve and the ratio of yields between 90- and 130-degree curves were also checked using nuclear track plates. Nine overlapping runs were made using several 14- and 24-kev thick targets at 130 degrees. Another run at 90 degrees, laboratory angle, was made, and the results plotted to the same relative scale for direct comparison of yields and resonances.

Figure 3 displays the data as center-of-mass cross section versus Bρ with all data points shown. Figure 4 displays the average 130-degree cross section and 90-degree cross section in laboratory coordinates with Rutherford cross sections shown for comparison.

TARGETS

The targets were SiO_2 on Formvar. Following a procedure suggested by Dr. C. K. Bockelman of Yale, SiO_2 in the form of quartz crystals was placed in a tantalum receptacle between electrodes and heated in a vacuum. A thin film of SiO_2 was uniformly evaporated on several layers of Formvar. Targets of various thicknesses were made in order to obtain a good compromise between resolution and counting rate.

The measured thickness of each target and the symbols used for data obtained from them on Figure 3 are tabulated below. The thickness shown is obtained by measuring the peak width at one-half the maximum peak height, for the peaks on the nuclear track plates.

From the known dispersion (21) and the quantities measured on the particular peak, the thickness in kev was easily determined.

TABLE I

Target	Thickness (kev)	Symbol on Figure 3.
SiO_2 No. 1	24	+ ǂ □
"C"	12	×
"F"	15	○ ▽ △
"G"	13	

○ (90° cross section only.)

III. THE COUNTER SYSTEM AND ITS CHARACTERISTICS

As used in this experiment, the counter system included:

1. The broad-range magnetic spectrograph.
2. The counter frame, which consists of
    (a) A 6199 RCA multiplier phototube operated at -500 volts with mu-metal shield.
    (b) A polished CsI(Tl) crystal 10 x 10 x 0.8 millimeters glued to the 6199 tube with araldite.
    (c) A lead shield.
3. A pulse amplifier and preamplifier, Model 100 (E3).
4. Two pulse counters, scale of 64 with built-in discriminators, Model 201 (E3).
5. A cathode-ray synchroscope.
6. Regulated DC (negative) power supply, -450 to -2000 volts (photomultiplier bias).
7. Target chamber current integrator (E2) with Faraday cage.

The magnetic spectrograph permits momentum selection of any desired reaction particle group at the fixed radius of the counter. The spectrograph is "tuned" for a particular $B\rho$ by a nuclear magnetic resonance fluxmeter. The spectrograph radius calibration is such that $B\rho$ is proportional to the Li^7 or proton Larmor frequency in the fluxmeters. Later, the frequency, or $B\rho$, width of the counter crystal aperture will be discussed.

In practice, depending upon the target and beam constituents, it is possible to have simultaneously alpha-particle, proton, and deuteron groups of the same Bρ incident on the counter crystal. Thus, further methods of discrimination are necessary. However, the momentum selection of the spectrograph considerably simplifies particle identification and makes precision pulse height discrimination equipment unnecessary.

By using a suitable target, it is only necessary to be able to separate alpha-particle, proton, and deuteron groups of equal Bρ and know or eliminate background, such as gamma pulses or random multiplier phototube "noise."

The counter frame, constructed for this experiment serves as a support for the lead shield of 3-cm average thickness and about 3π geometry relative to the cesium-iodide crystal. Before the lead shield was used, gamma background was a source of error in counting difficult to determine, because it depends on total beam current rather than integrated current through the target. With the lead shield, dense gamma pulse height was less than 30 percent of deuteron pulse height at the lowest beam energy used.

The characteristics of the cesium-iodide crystal (as mounted on the 6199 RCA multiplier phototube) are shown in Figure 1. These data were obtained by bombarding a thick (1 mm) gold target with alpha particles, protons, and deuterons. This thick target gave a continuous range of particle momenta from about zero to a maximum value determined by the input energy. By varying the spectrograph

field, different momenta particles are allowed to hit the scintillation crystal. The resulting pulses are observed in the cathode-ray synchroscope, and their height was measured by the scale on the cathode-ray tube face for each input Bρ.

Since the crystal aperture is finite (8 mm), the pulses are not truly monoenergetic, but this effect is small compared with the uncertainty of measured pulse heights. By counting the number of pulses per microcoulomb of incident beam versus Bρ, the edge of the thick gold target particle distribution was determined, and from this Bρ, the mean trajectory radius for the counter aperture was determined.

At the location of the counter in the spectrograph, the dispersion (Z1) is:

$$\frac{1}{E}\ \frac{dE}{dx} = 0.861\ \frac{\text{kev}}{\text{Mev mm}}, \text{ where} \qquad \text{(Eq. 1)}$$

dx refers to distance along the nuclear track plates usually used in the spectrograph.

The counter crystal is approximately perpendicular to the particles' trajectory; hence,

$$ds(\text{crystal}) = \frac{dx}{2.228}, \qquad \text{(Eq. 2)}$$

where 2.228 is the magnification caused by plate inclination (Z1) or

$$\frac{1}{E}\ \frac{dE}{ds} = 1.92\ \frac{\text{kev}}{\text{Mev mm}}. \qquad \text{(Eq. 3)}$$

Equivalent expressions are, for the counter (ds = 8 mm):

$$\frac{dE}{E} = 15.4 \ \frac{\text{kev}}{\text{Mev}} \qquad \text{(Eq. 4)}$$

$$\frac{\Delta(B\rho)}{(B\rho)} = 0.0077 = \frac{\Delta f}{f}, \qquad \text{(Eq. 5)}$$

where $\Delta f/f$ refers to the frequency of the nuclear magnetic resonance fluxmeter of the spectrograph.

The finite width of the counter aperture is necessary to insure that all the particles of the group being counted fall on the crystal. This was frequently checked by holding a constant input beam energy on the target and varying the spectrograph field to sweep the group across the crystal; a typical result is shown on Figure 2. The difference between the calculated and measured crystal width in units of $B\rho$ is caused by (1) finite target thickness, and (2) beam inhomogeneity, which is a fraction of one-half or less than target thickness.

From the above, two additional methods of discrimination are available:

1. Pulse height discrimination between deuterons and other particles.

2. The shape of the momentum distribution.

Method (1) is by far more sensitive, but is difficult when applied to separate deuterons and alpha particles, because of the small difference in pulse height, as seen in Figure 1. However, from

nuclear track plate data, the alpha yield, coincident with the $O^{16}(d,d)O^{16}$ elastic group, is less than 0.5 percent for the targets used. Figure 2 shows a typical momentum distribution for a single group of particles incident on the crystal.

In practice, data were taken by adjusting the spectrograph field to center the elastic deuteron group on the crystal and then setting the discriminators on the two pulse counters, such that counter No. 1 read deuteron and proton counts, but no gamma count, and counter No. 2 read only proton counts.

The discriminators were set by observing pulse height on the synchroscope after a proper choice of amplifier gain. The discriminator of counter No. 1 was modified to trigger the synchroscope only when pulses are counted, thus facilitating making discriminator settings. With proper discriminator settings, residual gamma background was less than 0.5 percent and was therefore neglected.

The Faraday cage used consists of an inner and outer cup, the outer cup being biased at -300 volts to repress secondary electrons.

The current to the outer cup was monitored and found to be directly proportional (1 percent) to the indicated beam current over a wide range of beam currents. The indicated microcoulomb exposure was therefore not absolute, but for all data taken is consistent to the accuracy of the electronic current integrator, which is 0.4 percent (E2).

Counting losses are considered negligible, since the maximum average counting rate never exceeded 20 counts per second with a pulse width of 2 microseconds.

IV. REDUCTION OF DATA

SUMMARY OF DATA

The data consisted of the following:

1. Nine overlapping sets of counter yield data, counts/microcoulomb versus (Bρ) of the deuteron beam at 130 degrees in the laboratory system.

2. Nuclear track plate No. 1388 with nine deuteron peaks at various (Bρ)'s in the laboratory system, using target SiO_2 No. 1. The angle of observation was 130 degrees.

3. One set of counter yield data, counts/microcoulomb versus (Bρ) at 90-degree angle of observation in the laboratory system.

4. Nuclear track plate data used to determine absolute cross sections. These data are shown in Table II. The peaks on the nuclear track plates used to determine cross sections were all placed at the same distance on the nuclear track plates to eliminate variation of solid angle, since laboratory solid angle is a function of spectrograph radius.

REDUCTION OF YIELD DATA

The data in items Nos. 1 and 2 above were taken at different times and, thus, had to be normalized to each other, since it was not always possible to duplicate target placement in the scattering chamber.

TABLE II

Summary of Plate Data

Plate No.	Zone	Yield	Incident E_{lab} (Mev)	θ_{lab}	Beam Par-ticle	Beam Par-ticle Energy in Mev	Expo-sure μc	Target
1499	30	d=1080	E_d=6.203	130°	d	6.203	100	F
	40	d= 58	E_d=6.005	130°	H_2^+	6.000	30	F
	50	p=5855	E_p=2.999	130°	H_2^+	6.000	40	F
1500	30	p=7559	E_p=2.999	130°	H_2^+	6.000	52	F
	40	d=1773	E_d=5.449	130°	d	5.449	40	F
	50	d=1571	E_d=6.203	130°	d	6.203	150	F
1501	30	d=1324	E_d=6.203	130°	d	6.203	150	G
	40	p=6094	E_p=2.999	122¼°	H_2^+	6.000	50	G
	50	d=1215	E_d=6.203	130°	d	6.203	150	G
1502	30	d=1906	E_d=5.449	130°	d	5.449	50	C(35°)
	40	d= 402	E_d=5.449	90°	d	5.449	50	C(35°)
	50	d= 368	E_d=5.449	90°	d	5.449	50	C(-45°)

One set of yield data, using target F, covered the entire range of (Bρ) without moving the target, although it was necessary to leave gaps in the yield data to cover this range in one run. This run was taken as the basis for normalizing the remaining data at 130 degrees.

Normalization to the above was accomplished by an integration process, after first reducing each run to a common microcoulomb exposure. All the points in common with the normalizing run were summed and then divided into the corresponding sum of the normalizing run. This ratio is the normalizing constant. Each point of the run was then multiplied by the normalizing factor and plotted.

For the average laboratory system cross-section curve, Figure 4 (Appendix I), all points at a given input (Bρ) have been averaged and the standard deviation computed by:

$$\sigma = \frac{1}{n - 1} \sqrt{\sum_i (x_i - \bar{x})^2} \qquad \text{(Eq. 1)}$$

except when n = 1; then:

$$\sigma = (\sqrt{\text{yield}}) \times (\text{normalizing factor}), \qquad \text{(Eq. 2)}$$

and when n = 2:

$$\sigma = \left(\frac{\text{range}}{2}\right). \qquad \text{(Eq. 3)}$$

For most points, $n > 3$.

The counter yield data at θ_{lab} = 90 degrees was obtained in one run at 50 microcoulomb exposure per point; hence, no self-normalization was necessary. It is, however, necessary to normalize the 90-degree laboratory system data to the 130-degree laboratory system data. This was accomplished by the data of plate No. 1502. From this plate, the ratio of laboratory cross section is:

$$\frac{\xi_{lab}(5.449 \text{ Mev}, \ 90^{\circ})}{\xi_{lab}(5.449 \text{ Mev}, \ 130^{\circ})} = \frac{402 \pm 20.5}{1906 \pm 43.7} = 0.211 \pm 5 \text{ percent.} \qquad \text{(Eq. 4)}$$

This ratio can be checked by counter data as follows, where Table III is composed of data from counter runs at the angles and energies shown.

TABLE III

Angle of Obs.	Target	Target Angle	Deuteron Yield Counts	Exposure μc	E_d (Mev)
130°	C	25°	653	20	5.449
90°	C	-45°	434	50	5.449

The factor to correct yield of target C from -45 to 25 degrees is:

$$\frac{\cos(-45^{\circ})}{\cos(25^{\circ})} = 0.7812. \qquad \text{(Eq. 5)}$$

The 90-degree yield corrected for target rotation = 340 counts. Then,

$$\frac{\xi_{\text{lab}}(5.449 \text{ Mev}, \ 90^{\circ})}{\xi_{\text{lab}}(5.449 \text{ Mev}, \ 130\ )} = \frac{(340 \pm 16.2)}{(653 \pm 25.5)} \cdot \frac{20\ \mu c}{50\ \mu c} = 0.208 \pm 6.7 \text{ percent.} \qquad \text{(Eq. 6)}$$

An average of these independent determinations gives:

$$\frac{\xi_{\text{lab}}(5.449 \text{ Mev}, \ 90^{\circ})}{\xi_{\text{lab}}(5.449 \text{ Mev}, \ 130^{\circ})} = 0.210 \pm 4 \text{ percent.} \qquad \text{(Eq. 7)}$$

It is also desirable to know this ratio in the center-of-mass system, which follows from:

$$\frac{\xi_{\text{CM}}(Ed_{\text{lab}}=5.449, \ \theta_{\text{lab}}= \ 90^{\circ})}{\xi_{\text{CM}}(Ed_{\text{lab}}=5.449, \ \theta_{\text{lab}}= 130^{\circ})} = \frac{\xi_{\text{lab}} \ 90^{\circ}}{\xi_{\text{lab}} \ 130^{\circ}} \cdot \frac{\left.\frac{d\omega}{d\Omega}\right)_{90^{\circ}}}{\left.\frac{d\omega}{d\Omega}\right)_{130^{\circ}}} =$$

$$(0.210)\left(\frac{1.0080}{1.1905}\right) = 0.178 \pm 4 \text{ percent} \qquad \text{(Eq. 8)}$$

where $d\omega$, the solid angle in the laboratory system, is constant.

CROSS-SECTION DETERMINATION

The absolute cross section was determined at two points on the 130-degree laboratory system yield curve by comparing the $O^{16}(d,d)$ yield with the $O^{16}(p,p)$ yield, for which the absolute cross section is known (E1).

The data from Eppling (E1) that was used is summarized in Table IV:

TABLE IV

$O^{16}(p,p)O^{16}$ Cross Sections

$E_{p_{lab}}$ in Mev	$\xi_{CM}(E_p, \theta_p)$ Milli-barns/ Steradian	θ_{CM}	θ_{lab}	ξ_{lab} Milli-barns/ Steradian
2.999	95.0*	125.30°	122.25°	88.9
2.999	93.0*	134.44°	131.71°	85.3

*± 1 percent

The following relation was used to determine the center-of-mass cross section of the $O^{16}(d,d)O^{16}$ data in millibarns/steradian:

$$\xi_{CM}(E_d, \theta_d) = \xi_{CM}(E_p, \theta_p) \frac{N_d \quad 2Q(H_2^+) \quad d\Omega_{CM}(\theta_p)}{N_p \quad Q_d \quad d\Omega_{CM}(\theta_d)}, \qquad \text{(Eq. 9)}$$

where N_d is the yield of deuterons for Q_d integrated current through the target.

The factor $(2Q_{H_2^+})$ arises, since a molecular hydrogen beam was used to get a proton energy in the range of Eppling's data.

$Q_{H_2^+}$, the integrated beam current, is subject to error from deuteron contamination of the beam. This has been measured by

observing the yield of $O^{16}(d,d)$ at the energy of the H_2^+ beam (nuclear track plate No. 1499); and, by computation, a figure of 9 percent contamination has been found (Appendix II).

This figure is at one hour after turning off the deuterium flow in the generator source. Since this contamination can be expected to approach zero after a sufficient length of time has elapsed, we have assumed:

$$Q_{H_2^+ (\text{actual})} = Q_{H_2^+ (\text{measured})} (1 - 0.045) \pm 5 \text{ percent.} \qquad (\text{Eq. } 10)$$

When yields at different angles are to be determined, it is necessary to bring the scattering chamber pressure to atmospheric in order to rotate the spectrograph. It has been noted that this increases the oxygen content of the target by about 10 percent. Hence, a relative yield determination must be a mean of several determination s. A method of avoiding this that has been used consists of assuming Eppling's data for 131.71 degrees in the laboratory system is equivalent to 130 degrees laboratory system, and this assumption has been used in obtaining the yield comparisons on nuclear track plates Nos. 1499 and 1500. The nuclear track plate No. 1501, however, was exposed at 122.25 degrees, laboratory angle, for the proton yield data to check the above assumption, and no significant difference was noted, except the effect of increasing oxygen in the target noted above. This averages out

to the first order, because the following exposure sequence was used for plate No. 1501:

1. Zone 30, $O^{16}(d,d)$ at 130 degrees
2. Open target chamber.
3. Zone 40, $O^{16}(p,p)$ at 122.25 degrees
4. Open target chamber
5. Zone 50, $O^{16}(d,d)$ at 130 degrees.

The results of the cross-section determination are shown below in Table V:

TABLE V

$E_{d_{lab}}$ in Mev	θ_{lab}	ξ_{CM} mb/ster.	Plate and Zone Number
6.203	130°	14.35	1499
6.203	130°	14.00	1500
6.203	130°	13.40	1501, Zone 50
6.203	130°	14.66	1501, Zone 30
5.449	130°	59.35	1500

The average center-of-mass cross section at 6.203 Mev and 130-degree angle of observation is:

$$\xi_{CM}(E_{d_{lab}} = 6.203,\ \theta_{lab} = 130^{\circ}) = 14.1 \text{ millibarns/steradian.}$$

Using this value and the relative yield for $E_d = 5.449$ Mev, we get

$$\xi_{CM}(5.449 \text{ Mev}) = 57.6 \text{ millibarns/steradian}$$

which is in good agreement with 59.35 millibarns/steradian in Table V.

Assuming a Poisson distribution in counting and knowing the uncertainty in the integrated H_2^+ beam, we assign a standard deviation of ± 0.7 millibarns/steradian to the above value of 14.1 millibarns/steradian.

The yield of deuterons at $\theta_{lab} = 130$ degrees, $E_d = 6.203$ averaged over four runs is 245 ± 4 counts for target F with 20 microcoulomb exposure. Hence, this is equivalent to 14.1 ± 0.7 millibarns per steradian; or the scale in the yield curves in the center-of-mass system is:

174.0 counts = 10 millibarns/steradian ± 5 percent,

and in the laboratory system is:

207 counts = 10 millibarns/steradian ± 5 percent.

ENERGY DETERMINATION

The magnetic spectrograph has been calibrated relative to polonium alpha particles. The calibration of the deflecting magnet has been determined relative to the magnetic spectrograph, and a radius of 60.51 cm was assigned.

The energy determination in this experiment depends on the calibration of the deflecting magnet, since the finite counter aperture precludes using the spectrograph to measure energies. Experience with the deflecting magnet indicates the precision of the deflecting magnet is 0.1 percent.

The Q-values of three excited levels of Si^{29} by a $Si^{28}(d,p)Si^{29}$ reaction have been measured. The Q-values were computed, using the beam energy as determined by the deflecting magnet. The values that were determined at $E_d = 6.203$ Mev agree within 5 kev with reported values, which had an uncertainty of ± 6 kev, and indicates that the deflecting magnet calibration has not changed. Therefore, we adopt 6 kev/6.2 Mev, which is about 0.1 percent as the precision of beam energy determination.

Examination of the center-of-mass cross-section curve shows that the peaks of resonances observed are displaced as much as 0.92 kilogauss-centimeters, which at 450 kilogauss-centimeters is 20 kev, and at 550 kilogauss-centimeters is 25 kev. This effect can be attributed primarily to differences in thickness of the various targets used and deflecting magnet hysteresis. The thick targets tend to average over rapid variations in yield. Therefore, the cross-section curves are drawn to conform to thin target points, and we adopt ± 10 kev as the standard deviation of resonance energies observed.

SUMMARY OF DATA REDUCTION AND ERROR DETERMINATIONS

The absolute cross sections of the 130-degree yield curves are given by:

174 counts = 10 millibarns/steradian ± 5 percent in center-of-mass system;

207 counts = 10 millibarns/steradian ± 5 percent in the laboratory system.

The ratio of the 90-degree yield curve to the 130-degree curve is 0.210 ± 4 percent in the center-of-mass system and 0.178 ± 4 percent in the laboratory system.

The 130- and 90-degree curves are self-consistent to the experimental errors displayed on the graphs.

For small stepwise changes in beam energy, as used in this experiment, energy differences are known to less than 0.1 percent. The absolute error is about 0.15 percent.

In resonance energy determinations, we have adopted a standard deviation of ± 10 kev for the range of excitation studied.

V. RESULTS AND CONCLUSIONS

The absolute cross section for the reaction $O^{16}(d,d)O^{16}$ at 130-degree angle of observation has been determined over the range of deuteron bombarding energies from 4.590 to 7.196 Mev, or 11.603- to 13.917-Mev excitation in the compound nucleus F^{18}, and at 90-degree angle of observation from $E_d = 5.449$ to 6.315 Mev.

The cross-section curves, Figures 3 and 4, display eight maxima, which are tabulated in Table VI. These peaks are superimposed on a background that has the appearance of a broad resonance peaked at $E_d = 5.5$ Mev with an estimated width of 730 kev. The fact that structure is observed in the yield curve is indicative of compound nucleus effects. At $E_d = 5.491$ Mev, a sharp increase in yield was observed, while using a target of 12-kev thickness, and must be regarded as an unexplained counting anomaly. Since this is the only "anomaly" observed, the cross sections are considered to show all resonance phenomena in this region of excitation of F^{18} with a resolution of 20 kev. Because points were taken about 20-kev apart, the net resolution is considered to be 40 kev.

If a broad resonance exists at about $E_d = 5.5$ Mev, we can estimate the widths of the peaks superimposed on this resonance by drawing an average curve along the base of the peaks, as shown in Figure 6. By this process, peak widths have been estimated for each of the eight maxima observed. These are shown in Table VI.

TABLE VI

Observed Maxima in $O^{16}(d,d)O^{16}$ Cross Sections

	130° Laboratory Angle				90° Laboratory Angle			
Peak No.	($B\rho$) kg-cm.	E_d Mev ± 10 kev	Excitation in F^{18} Mev	Γ (Est) kev	($B\rho$) kg-cm.	E_d Mev ± 10 kev	Excitation in F^{18} Mev	Γ (Est) kev
1	445.80	4.756	11.751	60				
2	460.98	5.084	12.042	25				
3	484.56	5.617*	12.516	136	**			
4	491.15	5.771	12.653	34	491.88	5.788	12.668	30
5	504.49	6.088	12.934	44	**			
6	517.29	6.401	13.212	90				
7	523.95	6.566	13.359	85				
8	530.64	6.735	13.509	62				

*±20 kev **not apparent

A broad resonance, as suggested by an average curve (Figure 6), is similar to the broad resonances in neutron cross sections calculated by Feshbach, Porter, and Weisskopf for the "Cloudy Crystal Ball Model."

Alternatively, the "background" may be the result of a dense level structure in the compound nucleus, such that the observed effect is a random combination of different angular distributions where certain levels have been emphasized by this reaction. For this interpretation, the data are insufficient to verify single levels or to assign level widths or spacings.

The shape of the yield curve at 90-degree angle of observation also suggests a broad level, peaked at $E_d = 5.7$ Mev with an estimated width $\Gamma = 440$ kev. The peak number 4 also appears on this background, and its estimated width agrees at the two angles of observation.

Further data at other angles of observation and for competing reactions in this range of excitation would be desirable to verify the resonance structure observed. This is particularly important in the region of peak number 1 where the shape of the cross section suggests interference phenomena for a single level. In particular, angular distribution data or, equivalently, the integrated cross section would resolve the question of dense versus resolvable level structure and permit definite energy-level assignments.

The marked decrease in cross section at 90-degree angle of observation (97.24°) center-of-mass system suggests that the cross section may be symmetric about 90 degrees, center of mass; however, as noted above, further work is necessary to verify this.

The data of Browne for the (d,α) reaction (B3)(B4) in Figure 5 show a pronounced asymmetric maximum peaked at $E_d = 6.370$ Mev, or 13.182-Mev excitation, which is within 30 kev of peak number 6 of the (d,d) data. These peaks may represent the same level in F^{18}. The 30-kev separation may be due to the difference in angles of observation; 30 degrees for the (d,α) reactions and 130 degrees for the (d,d) scattering. If the (d,α) data were integrated over the three alpha-particle groups observed, this peak would shift in the proper direction to lower the 30-kev difference.

If this resonance in the (d,α) data and the present work is actually an isolated level in F^{18}, then it is probably a $T = 0$ level.

In passing, one other relation between the $O^{16}(d,\alpha)N^{14}$ and the $O^{16}(d,d)O^{16}$ reactions should be noted. At $E_d = 6.222$ Mev, the minimum of the $O^{16}(d,d)O^{16}$ yield corresponds to a broad maximum in the alpha yield to the first excited state in N^{14} (which is a $T = 1$ state (A1)) and an irregularity in the broad maximum of the alpha yield going to the ground state of N^{14} (which is a $T = 0$ state (A1)). However, because of different angles of observation and unknown angular dependence of the cross section at this energy, it is not pos-

sible to draw any definite conclusions about level structure at this energy.

The results of this investigation clearly indicate the need for further work at both lower bombardment energies and at other angles of observation. If sufficient angular distribution data were taken in the presently investigated range of excitation, the integrated cross section for $O^{16}(d,d)O^{16}$ might reveal single levels that could then be compared with the $O^{16}(d,\alpha)N^{14*}$ reaction excitation functions, which should also be integrated over all angles of observation. At lower excitation energies, the work of Heydenburg and Inglis (H1) and Stratton et al (S1) is available on the excitation function $O^{16}(d,p)O^{17}$ where the ground-state protons in the above reaction show compound nucleus effects (A1). Further work at lower excitation energies in F^{18}, where levels could be expected to be isolated would probably be the more desirable alternative and facilitate isobaric spin assignments to the levels.

Figure 7 is drawn with the (d,α) and (d,d) results superimposed for the overlapping regions of excitation in F^{18}. The resonance structure is seen to show definite correlation.

APPENDIX I

NORMALIZED AVERAGE COUNTS DATA AT 120° [illegible] ANGLE

(Ep) [illegible]	[illegible]	Average Counts [illegible] [illegible] [illegible]
433.633	[illegible]	
437.935		[illegible] ± 26
438.849		[illegible] ± 17
439.764		650 ± 50
440.678		695 ± 25
441.592		725 ± 7
442.506		745 ± 17
443.421		751 ± 20
444.335		771 ± 11
445.249		906 ± 35
446.163		886 ± 5
447.078		872 ± 25
447.992		800 ± 35
448.906		720 ± 35
449.820		728 ± 12
450.735		683 ± 12
451.649		684 ± 14
452.563		656 ± 12
453.478		675 ± 32
454.392		667 ± 13

455.306		599 ± 43
456.220		638 ± 30
457.135	5000.00	612 ± 25
458.049		677 ± 9
458.415		724 ± 27
458.963		778 ± 31
459.877		876 ± 37
460.792		908 ± 24
461.706		887 ± 45
462.620		949 ± 18
463.535		1007 ± 18
464.449		1019 ± 33
465.363		1009 ± 33
466.277		1015 ± 17
467.192		1042 ± 26
468.106		993 ± 26
469.020		1025 ± 37
469.934		1033 ± 40
470.849		1028 ± 22
471.763		1001 ± 6
472.677		998 ± 14
473.591		1001 ± 41
474.506		1031 ± 21
475.420		1020 ± 24
476.334		1012 ± 43

477.248	5449.37	1002 ± 14
478.163		1000 ± 11
479.077		1020 ± 12
479.099		1237 ± 35
479.463	5500.00	
479.991		1092 ± 27
480.906		1136 ± 20
481.820		1164 ± 24
482.734		1211 ± 21
483.648		1252 ± 16
484.563		1239 ± 15
485.477		1239 ± 25
486.391		1208 ± 17
487.306		1163 ± 27
488.220		1097 ± 36
489.134		1064 ± 12
490.048		960 ± 21
490.963		989 ± 28
491.877		951 ± 33
492.791		926 ± 30
493.705		920 ± 21
494.620		810 ± 20
495.534		755 ± 25
496.448		713 ± 29
497.362		637 ± 20

498.277		579 ± 10
499.191		520 ± 10
500.105		540 ± 29
500.816	6000.00	
501.020		501 ± 12
501.934		481 ± 40
502.848		463 ± 9
503.762		475 ± 16
504.677		475 ± 18
505.591		461 ± 17
506.139		429 ± 16
506.505		430 ± 16
507.419		338 ± 21
508.334		293 ± 9
509.248		245 ± 4
509.614		229 ± 9
510.162		235 ± 12
511.077		263 ± 12
511.991		281 ± 6
512.905		302 ± 13
513.819		347 ± 34
		422 ± 20
514.734		425 ± 15
		521 ± 23

515.648		474 ± 27
		605 ± 25
516.562		588 ± 23
		611 ± 20
		632 ± 25
517.476		581 ± 11
		640 ± 25
518.391		540 ± 23
		547 ± 23
519.305		509 ± 5
		499 ± 40
520.219		481 ± 23
521.134		487 ± 13
521.301	6500.00	
522.048		541 ± 13
522.962		567 ± 7
523.876		569 ± 26
524.791		567 ± 18
		527 ± 23
525.705		535 ± 25
526.619		540 ± 12
527.533		533 ± 9
528.448		515 ± 10
529.362		519 ± 20

530.276		607 ± 28
531.190		591 ± 23
532.105		546 ± 45
533.019		546 ± 15
533.933		496 ± 16
534.848		437 ± 17
535.762		401 ± 17
536.676		362 ± 17
537.590		364 ± 17
538.505		371 ± 17
539.419		383 ± 17
540.333		405 ± 17
541.016	7000.00	
541.247		427 ± 18
542.162		487 ± 18
543.076		474 ± 18
543.990		496 ± 18
544.905		463 ± 18
545.819		484 ± 18
546.733		487 ± 18
547.647		492 ± 18
548.562		492 ± 18

Note: 174 counts = 1 millibarn/steradian in the center-of-mass system.

NORMALIZED AVERAGE COUNTER DATA AT 90° SPECTROGRAPH ANGLE

(Bρ) Kilogauss-Centimeters	E(in) kev	Average Counts per 50 μc Normalized to Target C
477.248	5449.39	434 ± 21
478.163		463 ± 22
479.077		490 ± 22
479.991		482 ± 22
480.906		550 ± 23
481.820		641 ± 25
482.734		724 ± 27
483.648		739 ± 27
484.563		738 ± 27
485.477		799 ± 28
486.391		835 ± 29
487.306		879 ± 30
488.220		878 ± 30
489.134		832 ± 29
490.048		856 ± 29
490.963		919 ± 30
491.877		988 ± 31
492.791		877 ± 30
493.705		788 ± 28
494.620		752 ± 27

495.534	684 ± 26
496.448	663 ± 26
497.362	592 ± 24
498.277	574 ± 24
499.191	548 ± 23
500.105	520 ± 23
501.020	528 ± 23
501.934	555 ± 24
502.848	565 ± 24
503.762	469 ± 22
504.677	481 ± 22
505.591	523 ± 23
506.505	487 ± 22
507.419	380 ± 19
508.334	417 ± 20
509.248	339 ± 18
510.162	312 ± 18
511.077	257 ± 16
511.991	194 ± 14
512.905	160 ± 13
513.819	151 ± 12

Note: These counts must be adjusted such that at (Bρ) = 477.25, the ratio of yields is 0.178 = Yield (90°)/Yield (130°) for proper center-of-mass ratios and 0.210 for the proper laboratory system ratio. In the center-of-mass system, 174 counts = 1 millibarn/steradian.

APPENDIX II

COMPUTATION OF DEUTERON CONTAMINATION IN MOLECULAR HYDROGEN BEAM

(From data of nuclear track plate No. 1499.)

1. Assume 130° lab $\approx$ 131.71° lab for $O^{16}(p,p)$ cross section.

2. $$\xi_d(6.203\ \text{Mev},\ 130^\circ)_{lab} = \xi_p(2.99\ \text{Mev},\ 131.71^\circ)_{lab}\ \frac{N_d}{N_p}\ \frac{2Q_{H_2^+}}{Q_d}$$

$$= 83.5\ \frac{1080}{5855}\ \frac{(2Q_{H_2^+})}{100} = 0.314\ Q_{H_2^+}\ .$$

3. We know that

$40\ \mu c = Q_{H_2^+} + Q_D$, where Q_D is the deuteron contamination of the muolecular hydrogen beam.

4. The yield of deuterons from contamination of the H_2^+ beam is

$$\left(58\ \frac{40\ \mu c}{30\ \mu c}\right) = 77.3 \text{ for } 40\ \mu c.$$

5. $$\xi_{lab_d}(6.005\ \text{Mev},\ 130^\circ) = \frac{500}{245}\ \xi_{lab_d}(6.203\ \text{Mev},\ 130^\circ),$$

where $\frac{500}{245} = 2.0325$ is the ratio of (deuteron) yields at the two energies involved.

$$6.\quad \frac{Q_d}{2Q_{H_2^+}} = \frac{N_d}{N_p} \cdot \frac{\xi_p(2.999\ \text{Mev},\ 131.71^\circ)_{lab}\ d\omega}{\xi_d(2.999\ \text{Mev},\ 130^\circ)_{lab}\ d\omega}$$

$$\frac{Q_d}{Q_{H_2^+}} = \frac{2(77.3)}{(5855)} \times \frac{(85.3)}{(2.0325)(0.3104)\ Q_{H_2^+}}\ .$$

Therefore,

Q_d = 3.52 microcoulomb contamination in 40 microcoulombs of molecular hydrogen beam one hour after shutting off deuterium beam, or

$$100\ \frac{3.52}{40} \approx 9\ \text{percent.}$$

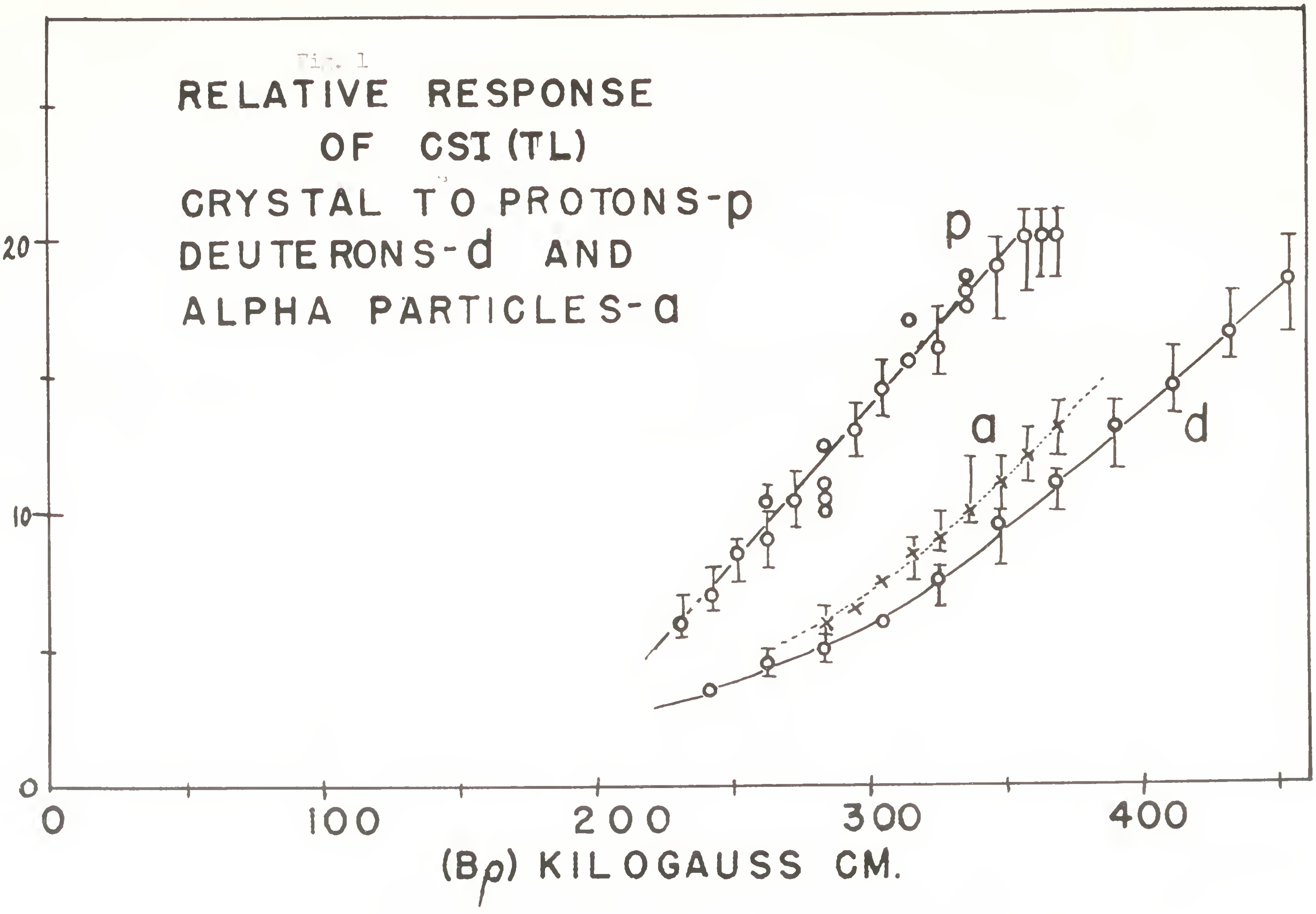

Fig. 1

RELATIVE RESPONSE
OF CSI (TL)
CRYSTAL TO PROTONS-p
DEUTERONS-d AND
ALPHA PARTICLES-a

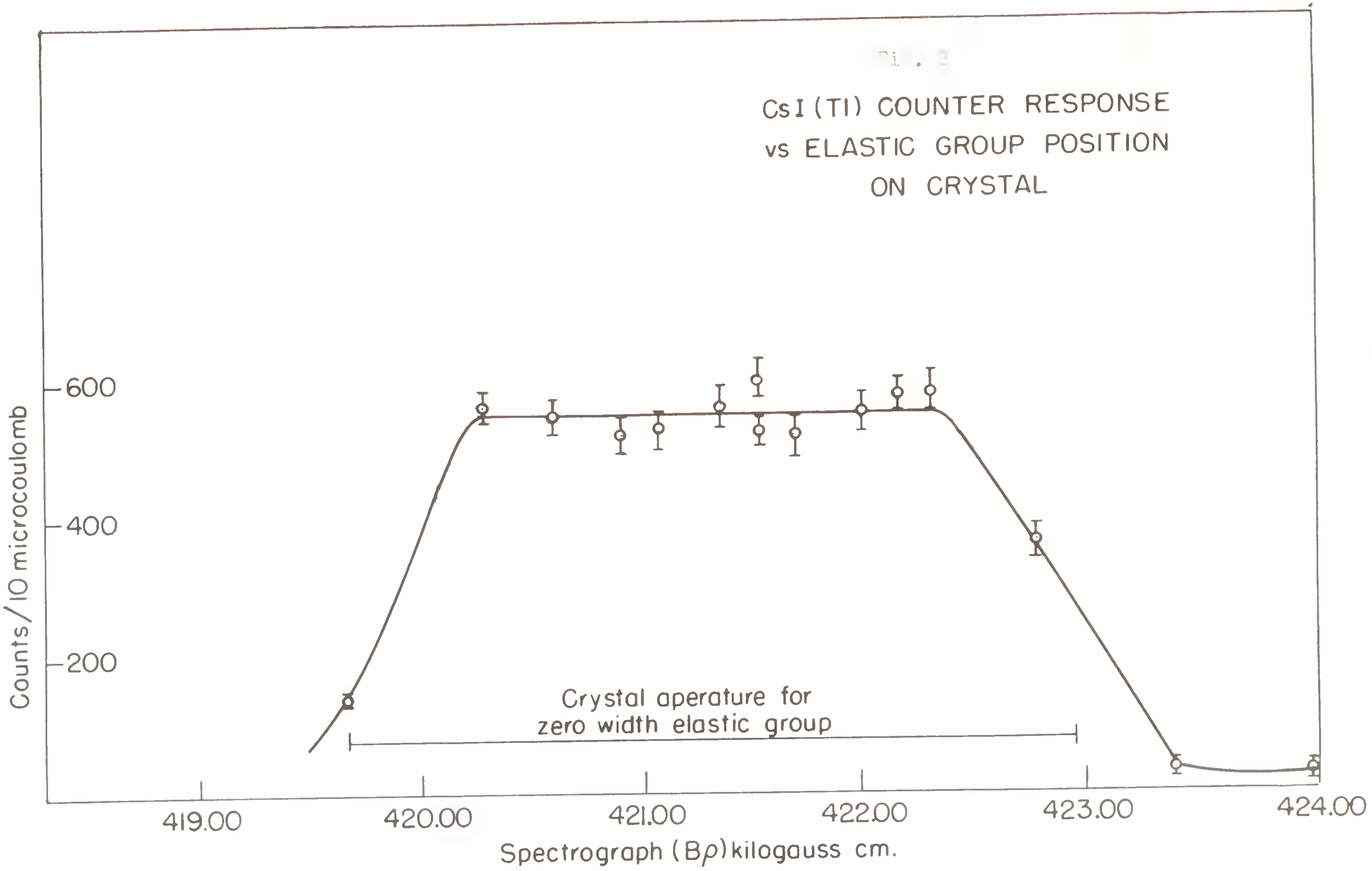

Fig. 3

CsI (Tl) COUNTER RESPONSE
vs ELASTIC GROUP POSITION
ON CRYSTAL

FIG. 3
CROSS SECTION FOR ELASTIC DEUTERONS FROM O^{16} AT 135.54° AND 97.24°
(Center of Mass)

(Deuteron energy and (Bρ) in laboratory)

○△▽× Thin Target Points ~ 14 kev (⊢)
‡ + ▫ Thick Target Points ~ 24 kev (⊢)
○ Nuclear Track Plate #1388 Thick Target
▨ Nuclear Track Plate #1500 Thin Target
135.54° C.M.
97.24° C.M.
Millibarns / Steradian Center of Mass
100
90
80
70
60
50
40
30
20
10
4500 kev
5000
5500
6000
6500
7000
440
450
460
470
480
490
500
510
520
530
540
550
(Bρ) Kilogauss centimeters

FIG. 4
CROSS SECTION FOR ELASTIC
DEUTERONS FROM O^{16}
(Laboratory)

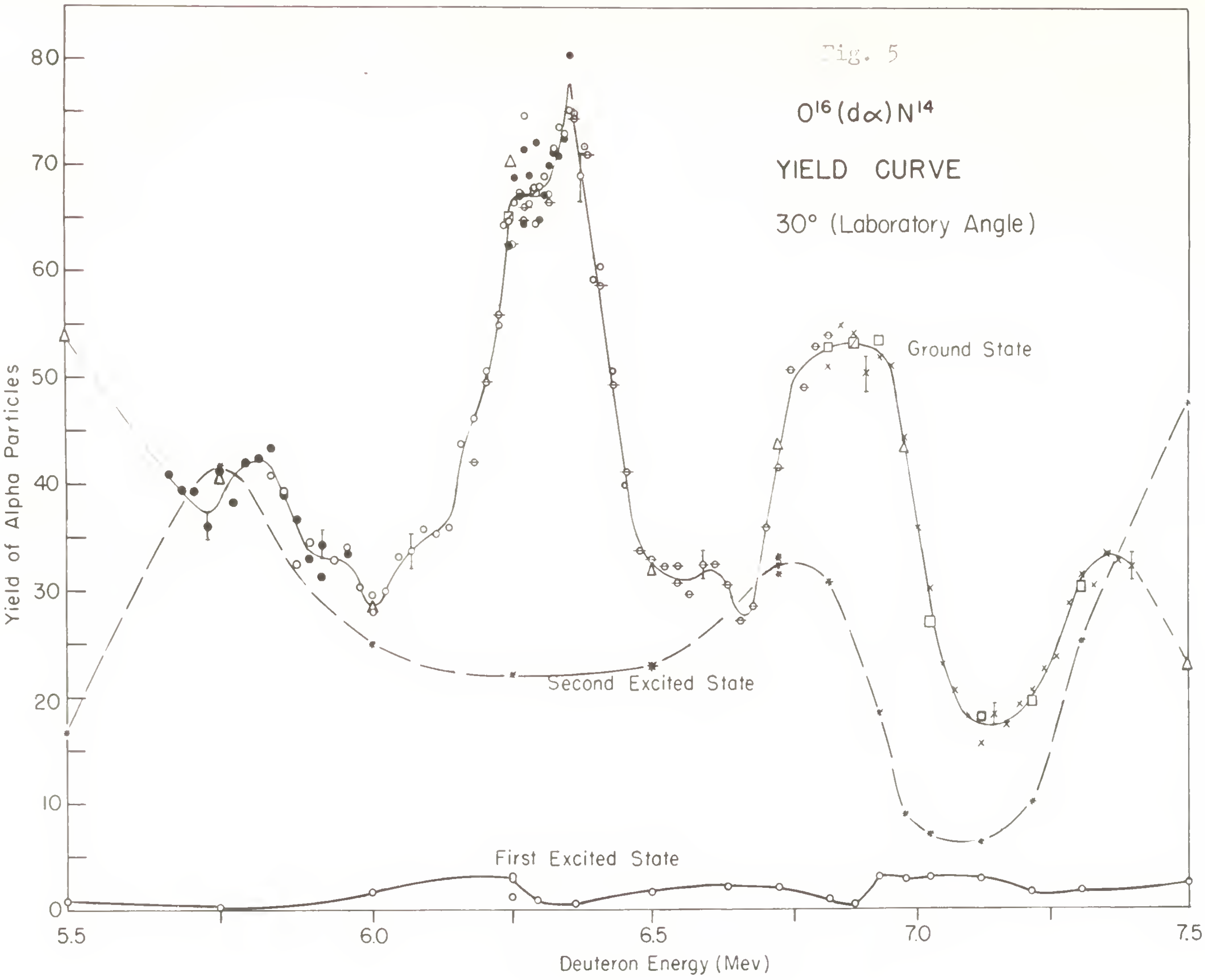
Fig. 5
$O^{16}(d\alpha)N^{14}$
YIELD CURVE
30° (Laboratory Angle)
Ground State
Second Excited State
First Excited State
Yield of Alpha Particles
Deuteron Energy (Mev)
0
10
20
30
40
50
60
70
80
5.5
6.0
6.5
7.0
7.5

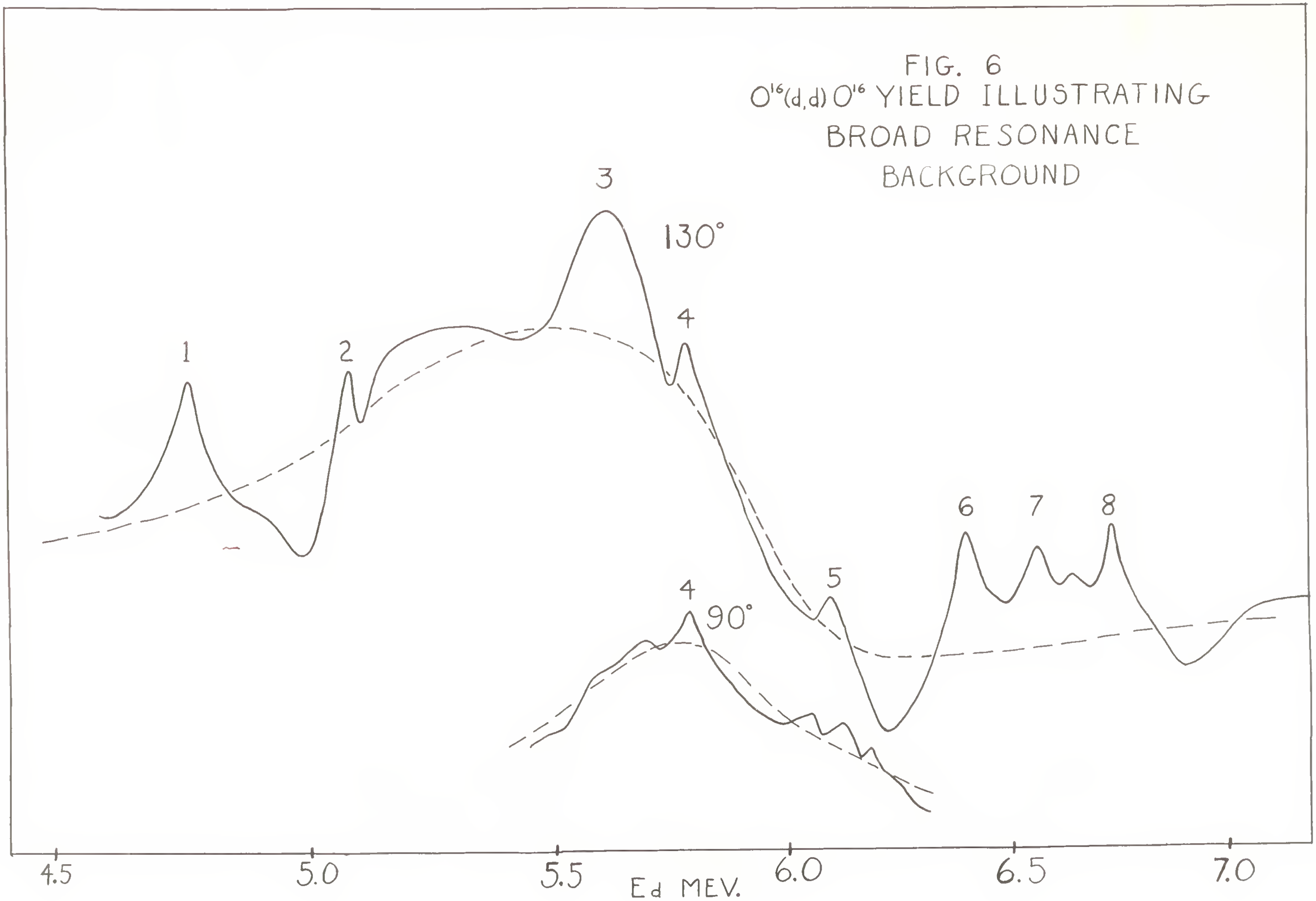

FIG. 6
$O^{16}(d,d)O^{16}$ YIELD ILLUSTRATING
BROAD RESONANCE
BACKGROUND

FIG. 7

Comparison of $O^{16}(d,d)O^{16}$ Yield at 130° with $O^{16}(d,\alpha)N^{14*}$ Yield at 30°

(vertical scale arbitrary) for each reaction

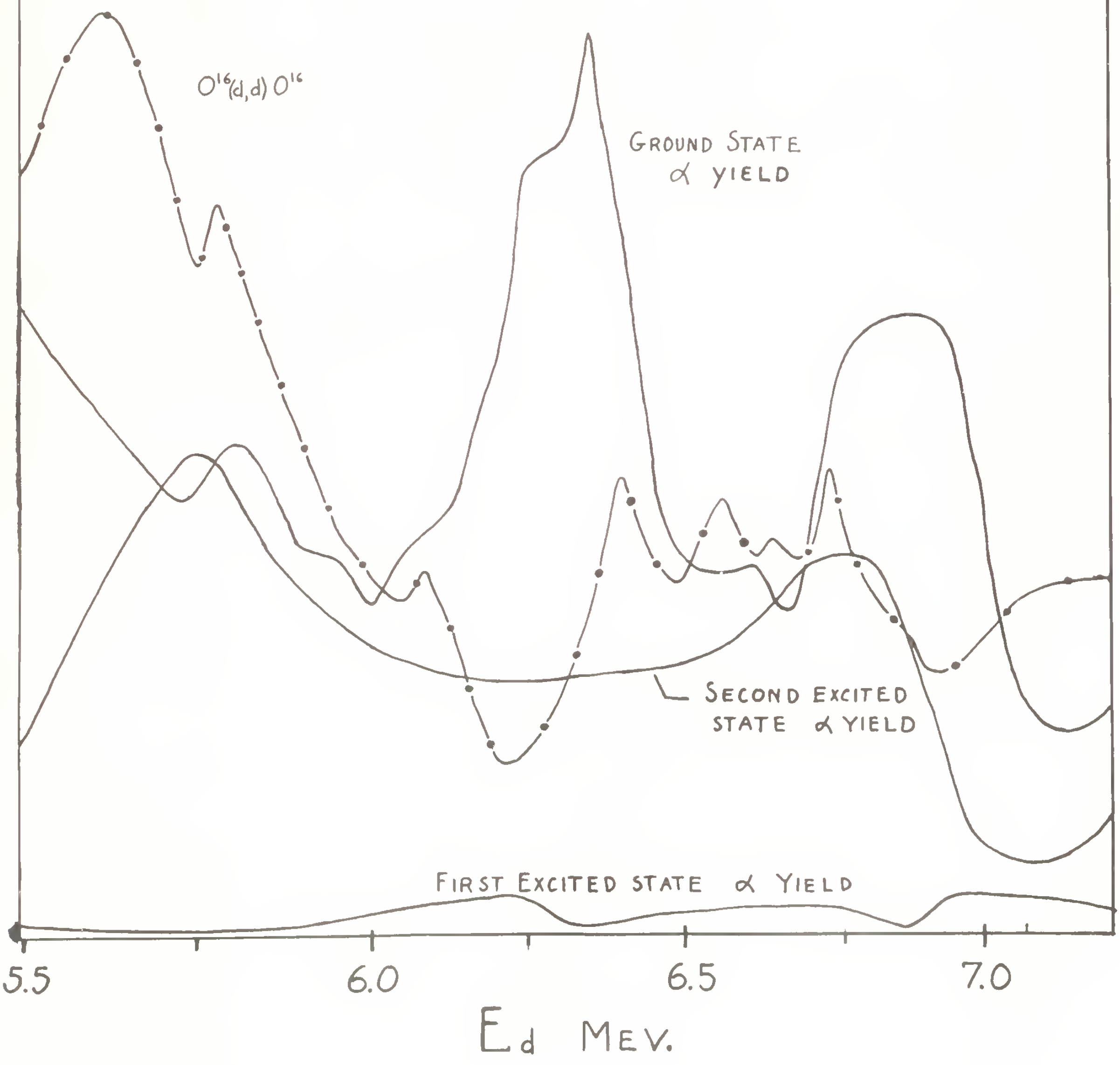

BIBLIOGRAPHY

(A1) F. Ajzenberg and T. Lauritsen, Revs. Modern Phys. 27, 77 (1955).

(B1) Buechner, Mazari, and Sperduto, Phys. Rev. 101, 188 (1956).

(B2) Buechner, Sperduto, Browne, and Bockelman, Phys. Rev. 91, 1502 (1953).

(B3) C. P. Browne, Phys. Rev. 100, 1253 (1955).

(B4) C. P. Browne, private communication, Figure 5, a continuation of the data from (B3).

(B5) T. W. Bonner and J. W. Butler, Phys. Rev. 83, 1091 (1951).

(E1) F. J. Eppling, "Elastic Scattering of Protons by O_2," Ph. D. Thesis, University of Wisconsin (1953). Also, private communication.

(E2) H. A. Enge, Rev. Sci. Inst. 23, 509 (1952).

(E3) W. C. Elmore and M. Sands, "Electronics, Experimental Techniques," National Nuclear Energy Series, Manhattan Project, Technical Section, Division V, Vol. I McGraw-Hill, (New York)(1949).

(H1) N. P. Heydenburg and D. R. Inglis, Phys. Rev. 73, 230 (1948).

(N1) H. W. Newson, Phys. Rev. 51, 624 (1937).

(S1) T. F. Stratton, G. M. Blair, K. F. Famularo, and R. V. Stuart, Phys. Rev. 98, 629 (1955).

(Z1) C. F. Zimmerman, Jr., "Focusing Properties of a High-resolution Magnetic Spectrograph," M. S. Thesis, M.I.T. (1955).

Thesis
B428 23008

Berger
Elastic scattering of
deuterons from O^{16}.

Thesis
B428 23008

Berger
Elastic scattering of deuter-
ons from O^{16}.

thesB428
Elastic scattering of deutrons from O(16
3 2768 002 13741 6
DUDLEY KNOX LIBRARY